IEEE Open Journal of
Circuits and Systems

Received 20 July 2022; revised 31 August 2022; accepted 6 September 2022. Date of current version 23 November 2022.

Digital Object Identifier 10.1109/OJCAS.2022.3206120

Droop-Controlled Bidirectional Inverter-Based Microgrid Using Cascade-Forward Neural Networks

MOHAMAD ALZAYED [1,2] (Member, IEEE), MICHEL LEMAIRE [1], SINA ZARRABIAN [3] (Member, IEEE), HICHAM CHAOUI [2] (Senior Member, IEEE), AND DANIEL MASSICOTTE [1] (Senior Member, IEEE)

[1] Laboratory of Signal and System Integration, Department of Electrical and Computer Engineering, Université du Québec à Trois-Rivières, Trois-Rivières, QC G9A 5H7, Canada

[2] Intelligent Robotic and Energy Systems Research Group, Department of Electronics, Carleton University, Ottawa, ON K1S 5B6, Canada

[3] Department of Electrical Engineering, State University of New York, Maritime College, Throggs Neck, NY 10465, USA

This article was recommended by Associate Editor M. Wang.

CORRESPONDING AUTHOR: M. ALZAYED (e-mail: mohamad.alzayed@uqtr.ca)

This work was supported in part by the Natural Sciences and Engineering Research Council of Canada Grant; in part by Prompt; in part by Opal-RT; in part by Hydro-Québec; in part by the Canada Foundation for Innovation; in part by CMC Microsystems; and in part by the Research Chair on Signal and Intelligent High-Performance Systems.

ABSTRACT The voltage source inverters in microgrids often rely on the droop control method integrated with voltage and inner current control loops in order to provide a reliable electric power supply. This research aims to present a Cascade-Forward Neural Network (CFNN) droop control method that manages inverter-based microgrids under grid-connected/islanded operating modes. The proposed method operates the inverter in a bi-directional technique for a wide range of battery energy storage systems or any other distributed generation systems. The proposed strategy uses the CFNN to learn the inverter's nonlinear model to achieve accurate demand and reference power tracking under different operating conditions for smart grid applications. Additionally, it reformulates the grid control concept to drive the inverter based on the optimal conditions by considering the power demand, reference power, equipment size, and disturbances. Also, it does not require any tuning procedure. The power tracking and operating performance of the proposed CFNN controller are evaluated through several experimental tests using the power hardware-in-the-loop (PHIL) methodology in different scenarios. All results are matched with the proven conventional strategy to confirm its effectiveness.

INDEX TERMS Distributed generation, droop control, inverter-based power system, microgrid, cascade-forward neural network.

NOMENCLATURE

LIST OF ACRONYMS

ACS	Average Current Sharing
CFNN	Cascade-Forward Neural Network
DER	Distributed Energy Resource
DG	Distributed Generation
FFNN	Feed-Forward Neural Network
GC	Grid-Connected
IS	Islanded/ off-grid
OPS	Optimal Power Sharing
PCC	Point of Common Coupling
RBFNN	Radial Basis Function Neural Network
SSN	State-Space Nodal
VSG	Virtual Synchronous Generator
VSI	Voltage Source Inverter

LIST OF SYMBOLS

L_c, R_c	Inverter-side series filter
L_g, R_g	Grid-side series filter
C_f	Parallel filter capacitor
v_i^{abc}, v_{dq}	Inverter-side 3-phase and dq voltage
i_i^{abc}, i_{dq}	Inverter-side 3-phase and dq current
v_c^{abc}	Mid-point filter voltage

v_g^{abc}, v_{gdq} Grid/load-side 3-phase and dq voltage
i_g^{abc} Grid/load-side current
v_{abc}^* Inverter reference 3-phase voltage

I. INTRODUCTION

DUE TO the devastating environmental impacts of conventional energy sources in existing electric power grids and growing global demand for decarbonizing electricity sector, high-level penetration of distributed energy resources (DERs) in the concept of microgrids has been considered predominantly in recent years [1], [2], [3]. Emerging technologies, developments, and advanced control in power converters have facilitated reliable integration of distributed generations (DGs) and local loads as a microgrid system that can supply the power in both grid-connected (GC) and off-grid (islanded) operating modes [3], [4].

Aside from their advantages, microgrids run into important challenges associated with the control of power converters. One of the main challenges in microgrids is balancing active and reactive power, known as power-sharing control, among multiple voltage source inverter (VSI)-based DGs in islanded mode and between grid and DERs in GC mode. Different inherent properties of the system such as load-generation mismatch due to intermittent operation of renewable resources, power converters' unequal capacity, unbalanced and nonlinear loads, and mismatch of power converters' equivalent output impedance can lead to a chaotic load sharing among power converters which in fact will result in serious voltage and frequency fluctuations, instability, and consequently a blackout. This issue can be addressed by precise control of inverters to ensure accurate load sharing and regulation of system frequency and voltage magnitude, especially in islanded operations [2], [5].

Among different approaches that contribute to regulating the exchange of active and reactive power in decentralized inverter-interfaced microgrids, increasing attention has been paid to droop control techniques in recent years [5], [6], [7]. It is noteworthy to mention that droop controllers are primary-level control units that are mostly implemented in grid-supporting converters to improve the stability of microgrid systems [8]. The common conventional droop-controlled inverters are operated based on active power-frequency droop control and reactive power-voltage magnitude of the point of common coupling (PCC) droop control. The principle concept of droop controllers in microgrids is similar to those utilized for synchronous generators. The droop control has gained popularity because of its advantages such as simplicity in implementation, adaptive adjustment of operating parameters, power-sharing regulation without enabling communication network among DERs, and high reliability [8], [9], [10]. On the other hand, the standard droop control mechanism encounters substantial limitations and deficiencies such as high frequency/voltage deviations, sensitivity to different DGs and network dynamic characteristics, lack of inertia support in highly power converter-integrated networks under disturbance, inaccurate power-sharing performance in low-voltage distribution systems with highly-resistive feeders or in medium-voltage grids with complex line impedance, and unsatisfactory slow transient response as well as instability issues [11], [12], [13], [14].

To overcome the aforementioned drawbacks and enhance the performance of the standard droop control, many novel approaches have been proposed. To tackle frequency fluctuations, angle droop control and virtual flux droop control methods have been proposed [15], [16], [17]. These methods achieve precise frequency control by direct adjustment of inverter voltage angle or virtual flux, but at the expense of GPS-based synchronization to ensure accurate initialization of angle among DGs. Nonlinear droop controllers have been introduced to address sensitivity of conventional droop control to different types of DGs and network dynamic characteristics [18], [19], [20], [21]. An improved droop control with a lead-lag compensation and virtual synchronous generators (VSGs) have been implemented in microgrid systems to cope with the lack of inertia pertaining to droop-controlled DGs [22], [23], [24], [25].

As pointed out previously, conventional droop controllers do not have satisfactory performance if used in predominantly-resistive distribution systems, in transmission lines with complex and unknown impedance, or grids with unknown line compensations. Additionally, observed impedance mismatch at parallel inverters' terminals has an adverse impact on droop controls. As a result, these conditions will cause imprecise power sharing and eventually instability. Since accurate active and reactive power sharing capability is critical for converter-controlled DGs and contributes significantly to a precise frequency and voltage regulation in microgrids, different modified droop control frameworks have been introduced to deal with this issue. A PSS-based droop control is introduced in [13] to enhance load sharing in inverter-based microgrids and achieve faster power sharing while maintaining low droop gains. However, it does not contribute to the reactive power sharing capability of the method. In another new approach [26], a universal optimal power sharing (OPS) method based on optimal power flow was utilized to optimize the droop settings of power converters for enhanced power sharing in a hybrid microgrid regardless of DG location and type. However, the OPS approach demands access to the load buses and the grid topology which increases the computation and communication burdens. In [27], a proportional-integral-based average current sharing (ACS) control with a small-signal model was embedded into the decentralized droop control to enhance power sharing performance in an islanded DC microgrid. However, the proposed model cannot eliminate the negative impact of feeder resistance variation on the damping ratio at dominant low-frequency modes.

The aforementioned approaches have some shortcomings such as lack of accurate decoupling of active and reactive power, dependency on topology and type of microgrids, and requirement for additional sensors and

measurements. Hence, some recent approaches aim at further enhancement of the droop controllers through intelligent control schemes [28], [29], [30], [31], [32], [33], [34]. Lin *et al.* [28] proposed a probabilistic wavelet fuzzy neural network algorithm to replace PI-based voltage controller in droop-controlled islanded microgrid for power sharing and load shedding purposes. Nevertheless, the execution time of the algorithm is long and the implementation is confined to a battery energy storage-based microgrid. In [29], a radial basis function neural network (RBFNN)-based hierarchical control framework is adopted for power sharing improvement in microgrid systems. This method adds a primary-level PI-based voltage control loop that uses the PIRBFNN technique to find reactive power references by solving power flow equations via the RBFNN technique as an additional loop to the hierarchical control scheme. This will eliminate the use of a low-pass filter in the droop control system. However, this method's accuracy relies highly on the proper tuning of the new PI controller which adds to the complexity of the system. Additionally, it does not provide the experimental implementation of the proposed approach and does not demonstrate the reactive power sharing accuracy of the proposed method. In [32], a data-driven intelligent control based on reinforcement learning is proposed to adapt virtual inertia emulation parameters for frequency control purposes. This paper mainly focuses on frequency control of microgrids rather than power sharing capability, and the proposed method is an offline model-based control scheme that requires a prior understanding of the system model. Authors in [34], proposed a data-driven online learning algorithm based on neural networks to replace the conventional hierarchical droop control framework for voltage/frequency regulation and power sharing control. The drawback of the method is that voltage regulation and reactive power sharing cannot be reached simultaneously and reactive power sharing is prioritized at the expense of higher voltage errors.

Unlike the approaches discussed earlier, the multi-layer cascade-forward back propagation method is suggested rather than the simplest and most common systems, such as the feed-forward multi-layer approach. The CFNN has the benefit of dealing with nonlinear relationships between input and output while leaving the linear relationship intact. Above that, an online neuron weights adaptation rule is applied to the error signals of the feedback values to close the loop and track the reference values according to the operating mode. Accordingly, in this research, a CFNN bi-directional technique that drives inverter-based microgrids is proposed to solve the limitations of: -tuning cascaded PI controllers; -individual tuning for different systems sizes; -the lack of accurate decoupling of active and reactive power in the conventional method; or -the calculation complexity in the other mentioned methods. The proposed method is built on top of a per-unit basis, which makes this method universal to apply to a wide range of inverter-based system sizes without any additional tuning. The bi-directional technique also gives beyond flexibility to integrate the BESSs into the grid. The online weights adaptation strategy gives an added value to the proposed system by tracking the reference active/reactive power in grid-connected mode or the nominal system voltage/frequency in the islanded mode.

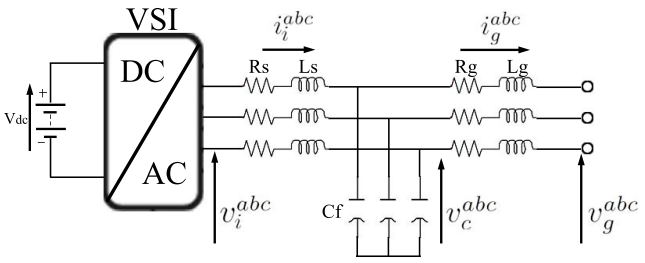

FIGURE 1. Three-phase VSI with LCL filter schematic diagram.

In summary, the paper's contribution is as follows:

- Presenting and training a universal cascade-forward neural network droop control system for driving bi-directional inverter-based microgrids. The suggested technique is based on the CFNN structure and the mathematical model of the microgrid droop control system.
- Online adapting of the neural network neuron weights pushes the feedback errors to zero, which helps the proposed method track the reference values in any operating mode with less deviation.
- The CFNN bi-directional inverter control technique avoids the limitations of tuning cascaded PI controllers, independent tuning for different systems sizes, lack of balancing of active and reactive power sharing, and calculation complexity.
- The effectiveness of the suggested method is proven through several PHIL experimental evaluations on 10KW, 100KW, and 1MW BESSs over a MATLAB/RT-Lab real-time environment software integrated with an Opal-RT processor *OP*4510. Accordingly, the presented scheme is validated and compared with the justified conventional strategy, which reveals the performance of the proposed approach in islanded and grid-connected operating modes.

Section II presents an analysis of the conventional droop control concept in microgrids. In Section III, the proposed CFNN is designed and implemented for bi-directional inverter-based microgrid systems. The PHIL experimental and simulation results for the proposed and conventional methods are offered in Section IV. Section V brings the investigation to a close with a concise overview and a clear solution.

II. DROOP CONTROL CONCEPT IN MICROGRIDS: MODELING AND FORMULATION

In modern grids, the voltage source inverters are used to integrate the distributed generation sources as well as the battery energy storage systems. Besides, the VSI is connected with an LCL filter, considered an interface device. Fig. 1 presents the energy source, VSI, and LCL filter. L_c, R_c

are the inverter-side series filter (series inductor and resistor). C_f is the parallel filter capacitor. L_g, R_g are the grid-side series filter's inductor and resistor. i_i^{abc}, i_g^{abc}, v_i^{abc}, v_c^{abc}, and v_g^{abc} are the inverter-side current, the grid-side current, the inverter-side voltage, the voltage of the filter mid-point, and the grid/load voltage in GC/IS mode, respectively. The conventional control structure for VSI-based microgrids consists of a droop control loop, voltage regulation control loop, and current regulation control loop. The conventional control technique presented by [8] is used as a benchmark model and discussed to build the mathematical control model. According to Fig. 1, the standard control framework is formulated in the synchronous reference frame, and the inner control loops are discussed as follows.

A. DROOP CONTROLLER MODELING

Droop controller in microgrids is classified as a primary-level controller that is implemented to each VSI for adjusting active and reactive power through reference frequency and magnitude of the inverter's output voltage. The standard droop control can be formulated as,

$$\omega = \omega_o + k_p\left(P^{ref} - P^{act}\right) \tag{1a}$$

$$E = E_o + k_q\left(Q^{ref} - Q^{act}\right) \tag{1b}$$

where ω and E are the angular frequency and magnitude of the inverter's output voltage reference, ω_o and E_o are the nominal/reference values of angular frequency and voltage magnitude, k_p and k_q are the droop controller gains, P^{act} and Q^{act} are the measured active and reactive power, and P^{ref} and Q^{ref} are active and reactive power reference values, respectively. Moreover, active and reactive power of the converter output can be obtained as,

$$P = \frac{\omega_f}{s+\omega_f}\left(v_d i_d \; + \; v_q i_q\right) \tag{2a}$$

$$Q = \frac{\omega_f}{s+\omega_f}\left(v_q i_d \; - \; v_d i_q\right) \tag{2b}$$

where ω_f is the cut-off frequency of the low-pass filter, and v_{dq} and i_{dq} are the inverter output voltage and current after transformation to the dq synchronous reference frame, respectively.

B. VOLTAGE AND CURRENT REGULATOR CONTROL LOOPS

The key feature of the voltage and current regulator control loops is to substantially enhance the voltage profile of microgrids in GC and IS operational modes. The outer control loop contains the voltage regulator block to adjust the power converter's output voltage. In this control loop, the voltage error signal is the input to a PI controller and the controller output generates the reference current to be used in the current regulator control loop. It is noteworthy to emphasize that the voltage regulation control loop is activated only in the off-grid (islanded) operation. The mathematical equations of the voltage control loop are written as,

$$i_d^{ref} = K_{p1}\; e_{v_d} + K_{i1}\int e_{v_d} \tag{3a}$$

$$i_q^{ref} = K_{p2}\; e_{v_q} + K_{i2}\int e_{v_q} \tag{3b}$$

where, $e_{v_d} = v_d^{ref} - v_{gd} = E - v_{gd}$, $e_{v_q} = 0 - v_{gq}$, $v_{g_{dq}}$ is the grid-side voltage in dq, i_{dq}^{ref} is the current reference in dq, K_{p1} and K_{p2} are the proportional gains of the PI controllers, and K_{i1} and K_{i2} are the integral gains of the PI controllers, respectively. The inverter output voltages v_{dq} are written as (4),

$$v_d = v_{gd} + Ri_d^{ref} + L\frac{d}{dt}i_d^{ref} - \omega L i_q^{ref} \tag{4a}$$

$$v_q = v_{gq} + Ri_q^{ref} + L\frac{d}{dt}i_q^{ref} + \omega L i_d^{ref} \tag{4b}$$

where, $R = R_c + R_g$ and $L = L_c + L_g$. In addition to the voltage control loop, the inner control loop consists of the current regulator block. The inner current control loop functions as the power converter current regulator while it receives the difference between the measured and reference current as the error signal and tracks the reference current fed by the voltage regulator loop through a PI controller. From (4a) and (4b), the voltage control loop integrated with the inner current control loop can be reformulated as,

$$v_d = v_{gd} + Ri_d^{ref} - \omega L i_q^{ref} + K_{p3}\; e_{i_d} + K_{i3}\int e_{i_d} \tag{5a}$$

$$v_q = v_{gq} + Ri_q^{ref} + \omega L i_d^{ref} + K_{p4}\; e_{i_q} + K_{i4}\int e_{i_q} \tag{5b}$$

where, $e_{i_d} = i_d^{ref} - i_d$ and $e_{i_q} = i_q^{ref} - i_q$. K_{p3} and K_{p4} are the proportional gains of the PI controllers, and K_{i3} and K_{i4} are the integral gains of the PI controllers, respectively.

C. ACTIVE AND REACTIVE POWER REGULATOR CONTROL LOOPS

The concept of active and reactive power sharing in microgrids via droop control strategy is derived from the emulation of $P-f$ and $Q-V$ droop regulations in synchronous generators. This is achieved by adjustment of active and reactive power in order to control grid frequency and voltage magnitude, respectively. In the active power control loop, the active power error signal is the input to a PI controller whose output generates reference current in the d-axis. Likewise, the reactive power control loop is fed by the reactive power error signal which is routed to a PI controller whose output establishes reference current in the q-axis. These reference currents in conjunction with the voltage control loop output are utilized in the current regulator control loop. As a result, the active and reactive power equations can be obtained as,

$$i_d^{ref} = K_{p5}\; e_P + K_{i5}\int e_P \tag{6a}$$

$$i_q^{ref} = K_{p6}\; e_Q + K_{i6}\int e_Q \tag{6b}$$

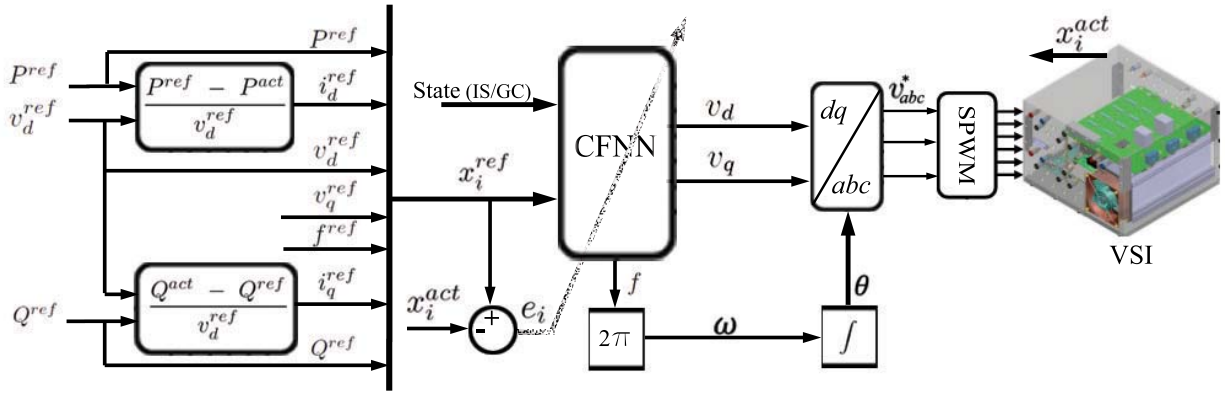

FIGURE 2. Bi-directional Inverter-Based Microgrid Cascade-Forward Neural Network Control Block Diagram.

where, $e_P = P^{ref} - P^{act}$, $e_Q = Q^{ref} - Q^{act}$, K_{p5} and K_{p6} are the proportional gains of the PI controllers, and K_{i5} and K_{i6} are the integral gains of the PI controllers, respectively.

III. CFNN-CONTROLLED BI-DIRECTIONAL INVERTER-BASED MICROGRID

Fig. 2 shows the control diagram of the CFNN-Controlled bi-directional inverter-based microgrid strategy that is presented along with this study. It includes a three-phase voltage source inverter and a CFNN droop controller for microgrid applications.

A. CASCADE-FORWARD NEURAL NETWORK

Neural networks are utilized for estimating, modeling, and control, most often in systems with a lack of knowledge on system behaviour, complexity, and dynamics. To achieve output goal values, neural networks possess training ability and parallelization. According to the neural network universal approximation theorem [35], neural networks can accurately approximate any nonlinear/dynamic characteristics. Rather than the simplest and common systems, such as the feed-forward multi-layer approach, the multi-layer cascade-forward back propagation method is suggested in this study. The CFNN has the benefit of dealing with nonlinear relationships between input and output while leaving the linear relationship intact. The relationship between the CFNN's inputs and outputs is described as follows,

$$\varphi_j^{(1)} = b_j^{(1)} + \sum_{i=1}^{m} \hat{w}_{ji}^{(1)} x_i \tag{7a}$$

$$O_j^{(1)} = f_j^{(1)}\left(\varphi_j^{(1)}\right) \tag{7b}$$

$$\varphi_j^{(h)} = b_j^{(h)} + \sum_{p=1}^{h-1}\sum_{k=1}^{n} O_{jk}^{(p)} w_{jk}^{(p)} + \sum_{i=1}^{m} \hat{w}_{ji}^{(h)} x_i \tag{8a}$$

$$O_j^{(h)} = f_j^{(h)}\left(\varphi_j^{(h)}\right) \tag{8b}$$

where, x_i is the input signal for m parameters, $\hat{w}_{ji}^{(h)}$ is the adapted linking weight of node j for input i of layer (h), $b_j^{(h)}$ is the bias of node j of layer (h), $f_j^{(h)}$ is the activation function of node j of layer (h), and $O_j^{(h)}$ is the j^{th} node's output signal of layer (h). Layer index 1: 1^{st} hidden layer, h: h^{th} hidden layer, and o: output layer. n: neurons' number. Lastly, the CFNN output signals $\hat{y}$ can be declared as $\hat{y} = [y_1, y_2, \ldots, y_l]$, where l is number of output signals.

The CFNN weights adjustment terms are learned using the back-propagation approach. The robustness of the closed-loop control system is then maintained by the online weights adaptation law, which is as follows,

$$\hat{w}_{ji}^{(h)} = w_{ji}^{(h)} + e_i w_{ji}^{(h)} \tag{9a}$$

$$\hat{y} = f_l^{(o)}\left(b_l^{(o)} + \sum_{p=1}^{h-1}\sum_{k=1}^{n} O_{jk}^{(p)} w_{jk}^{(p)} + \sum_{i=1}^{m} w_{ji}^{(o)} x_i + \sum_{i=1}^{m} e_i w_{ji}^{(o)} x_i\right) \tag{9b}$$

where, $e_i = x_i^{ref} - x_i^{act}$, e_i is neural network's input signal (i) feedback error, x_i^{ref} is reference value, and x_i^{act} is actual value of the neural network's input signal (i).

The proposed CFNN is composed of four layers as shown in Fig. 3. Input layer (1^{st} layer) of twenty-four neurons is used to hook the input parameters (i.e., P, Q, v_d, v_q, f, i_q, i_d, and operational state), sixteen neurons for the second hidden layer, eight neurons compose the third hidden layer, and three neurons shape the output layer (i.e.,v_d, v_q, and f). The Tan-Sigmoid function in (10a) is used as activation function for 1^{st}, 2^{nd} and 3^{rd} layer, and the output neuron (4^{th}) layer uses a Purelin transfer function, written in (10b).

$$f_{TS}^{(1,2,3)}(x) = \frac{2}{1 + e^{-2x}} - 1 \tag{10a}$$

$$f_P^{(o)}(x) = x \tag{10b}$$

The conventional control mathematical model (Section II) is used to generate the neural network training data. The load and reference active power (P) and reactive power (Q) are modified in the mathematical application within the ranges of $[-1\ 1]$ (pu) and $[-0.6\ 0.8](pu)$, with increments of $1 \cdot 10^{-3}(pu)$ and $2 \cdot 10^{-3}(pu)$, respectively. The reactive

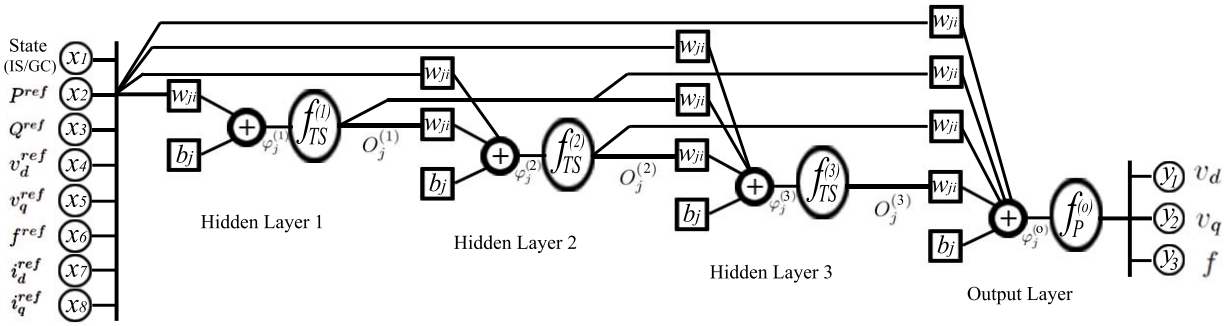

FIGURE 3. Proposed Cascade-Forward Neural Network scheme.

power range is chosen based on its physical characteristics, leading/lagging operating, and avoiding a power factor of less than 0.8. Also, from the model of $P-f$ and $Q-V$ droop regulators in synchronous generators and with the knowledge of a wide regulation range of voltage than frequency, the P increment step is selected with a value smaller than the Q step. The mathematical application results are utilized to create the learning data matrix. The mean square error (MSE) target is defined as $0.5 \cdot 10^{-3}$, which equals half of the active power increment and one-fourth of the reactive power increment. The goal of using CFNN is to reach the target mean square error faster than the FFNN and make the output signals more robust against the neural network's input signals variations, [36].

B. CASCADE-FORWARD NEURAL NETWORK BI-DIRECTIONAL INVERTER-BASED GRID CONTROLLER

Understanding the relationship between the voltage v_{dq} and the load/reference power helps extract an accurate control model for grid inverter-based controller. The proposed model operates the VSI in islanded and grid-connected modes for microgrid applications. It can drive the inverter to supply a standalone load (islanded mode) or connect in parallel with another inverter or AC grid to supply the loads with the required power as per the reference active and reactive power in two directions (microgrid system). The proposed technique gives flexibility to grids and loads to manage their energy.

The control voltage v_{dq} and frequency/angular velocity f/ω can be provided through the neural network implemented control scheme without any of the conventional control loops (droop, voltage, and inner current loops). This can be achieved by generating dq-axes voltages and frequency that are needed to provide the required voltage amplitude and angle for maintaining the supplied/demand power.

The CFNN's input signals are assigned through the reference active/reactive power P^{ref}, Q^{ref}, reference current i_{dq}^{ref}, reference voltage v_{dq}^{ref}, reference frequency f^{ref}, and operational mode (islanded or grid-connected). Further, the reference current i_{dq}^{ref} is calculated based on the reference/actual active/reactive power and reference voltage as,

$$i_d^{ref} = \frac{P^{ref} - P^{act}}{v_d^{ref}} \tag{11a}$$

$$i_q^{ref} = \frac{Q^{act} - Q^{ref}}{v_d^{ref}} \tag{11b}$$

The offline training technique is used to train the proposed cascade-forward neural network based on the data built through the conventional control mathematical model (Section II). To minimize unexpected errors generated by approximations and voltage source inverter nonlinearity, and to compensate for the residual errors, a feedback signal is needed. A closed-loop control system is also required to compensate for the discrepancy between the reference values and actual values of the voltage and frequency or active/reactive power caused by losses. As a result, $e_P = P^{ref} - P^{act}$, $e_Q = Q^{ref} - Q^{act}$, $e_{v_d} = v_d^{ref} - v_d^{act}$, $e_{v_q} = v_q^{ref} - v_q^{act}$, $e_{i_d} = i_d^{ref} - i_d^{act}$, $e_{i_q} = i_q^{ref} - i_q^{act}$, and $e_f = f^{ref} - f^{act}$ determine an active power, reactive power, v_{dq} voltage, i_{dq} current, and frequency feedback errors (e_i). To drive these errors to zero, an online neuron weights adaptation rule is used. As a result, the current is controlled indirectly. The proposed method is built on a per-unit basis, which makes this method universal to apply to a wide range of inverter-based system sizes without additional tuning. The communication system helps transmit the reference values (P, Q) and operating mode/state (islanded or grid-connected) from the command/dispatch center to the proposed inverter's control system.

As shown in Fig. 2, the control voltage v_{dq} and frequency are sent to a sinusoidal pulse width modulation (SPWM) for delivering the proper inverter pulses through Park transformation v_{abc}^*.

IV. PHIL EXPERIMENTAL VALIDATION

A. MICROGRID TEST CIRCUIT

The proposed strategy is designed to be a universal bi-directional CFNN droop controller; therefore, the test circuit is implemented to cover most operating conditions and confirm the effectiveness, robustness, and practical use of the proposed method. The test circuit, Fig. 4, contains three different sizes of voltage source systems 10KW, 100KW, and 1MW. Each of them is connected to a battery storage system on the DC side, and an LCL filter and isolation

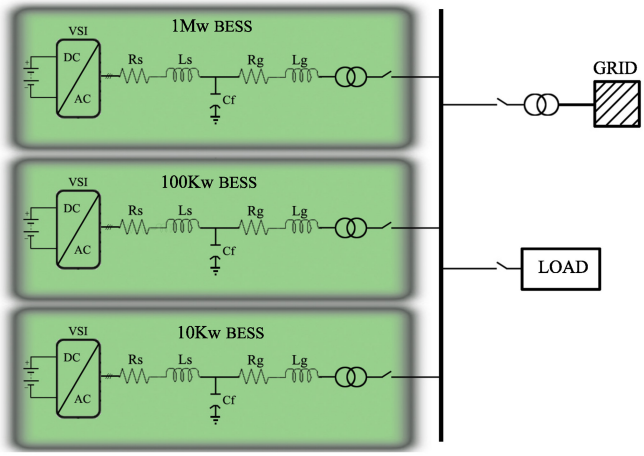

FIGURE 4. Microgrid test circuit scheme.

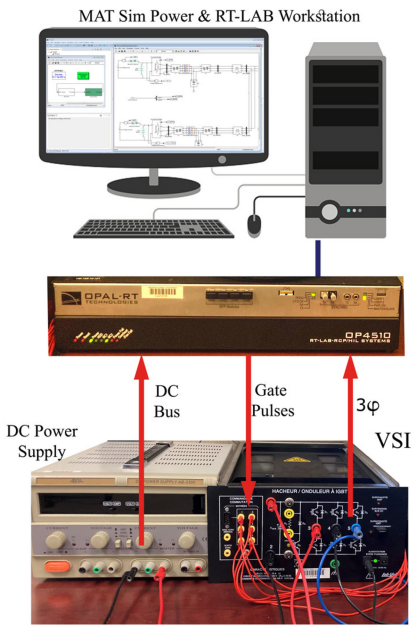

FIGURE 5. PHIL Experimental setup.

transformer on the AC side. A wide range of active/reactive loads and a grid model are attached to the main bus to validate the circuit in islanded and grid-connected mode.

B. PHIL EXPERIMENTAL SETUP

The experimental evaluations are carried out on a power-hardware-in-the-loop (PHIL) setup [37] to emphasize the effectiveness of the Cascade-Forward Neural Network control methodology. The PHIL system consists of a LabVolt 3-phase IGBT-based voltage source inverter, a voltage power source and a *OP*4510 real-time simulator, as shown in Fig. 5. The LCL filter, loads, microgrid and power electronic circuit are implemented using MATLAB Simulink SimPowerSystems and Artemis library [37]. The state-space nodal (SSN) approach is necessary to decouple the electric circuit simulation since the overall system contains too many switches [38], [39].

TABLE 1. Power system parameters.

Parameter	Value
DC Voltage (V)	$v_{dc} = 922$
Nominal grid/load frequency (Hz)	$f = 60$
Nominal grid/load L-L voltage (V)	$v_{rms} = 600$
Inverter-side filter (mH, Ω)	$L_s = 0.7,\ R_s = 2.63 \cdot 10^{-4}$
Parallel filter (KVAR)	$Q_{C_f} = 50$
Grid-side filter for 1MW BESS (H, Ω)	$L_g = 0.06,\ R_g = 0.003$
Grid-side filter for 100KW BESS (H, Ω)	$L_g = 0.3,\ R_g = 0.015$
Grid-side filter for 10KW BESS (H, Ω)	$L_g = 0.35,\ R_g = 0.02$

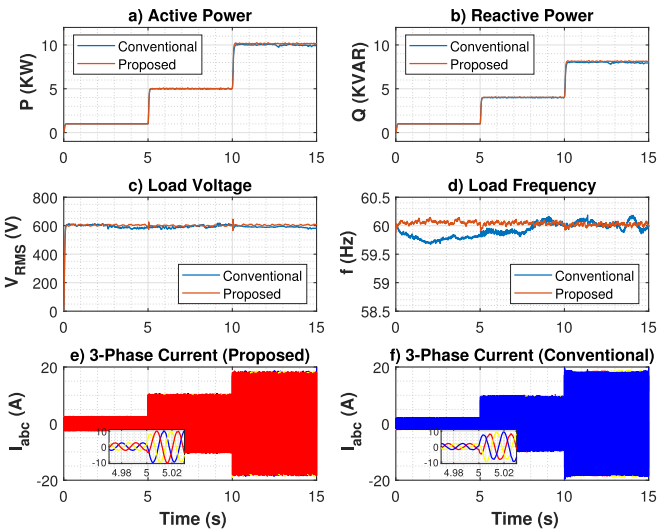

FIGURE 6. PHIL experimental results for 10KW system at IS mode.

The introduced control scheme, including the CFNN, is built in a high-level real-time platform using a MATLAB s-function with a time-step of the simulation of $40\mu s$. The driving pulses are generated using Opal-RT Technologies, RT-EVENT library block [40], at a switching frequency of $2.7kHz$. Thanks to the digital outputs of the simulator that are used to interface with the VSI gates inputs. The inverter phase-to-phase voltage output is directly measured using the analog input of the *OP*4510. The physical BESS consists of a DC power supply and VSI, scaled to $922VDC$, 10KW, 100KW, or 1MW. The parameters of the power system and LCL filters are listed in Table 1.

C. ISLANDED MODE

In this test, each voltage source system feeds its related load, dependent on the size of the system separately. Fig. 6, 7 and 8 present PHIL experimental results for the CFNN method and conventional method under load variation for 10KW, 100KW, and 1MW systems, respectively.

1) 10KW SYSTEM

In Fig. 6, the load active power changes from zero to 1KW, 5KW till 10KW, and the load reactive power varies from zero to 1KVAR, 4KVAR till 8KVAR. The frequency and voltage curves, Fig. 6(d), (c), reflect to what extent the proposed method can deliver the required active/reactive power at the nominal system parameters of the frequency

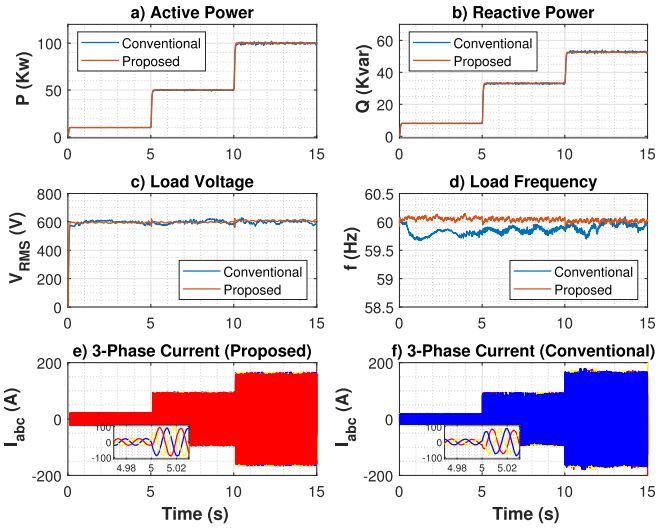

FIGURE 7. PHIL experimental results for 100KW system at IS mode.

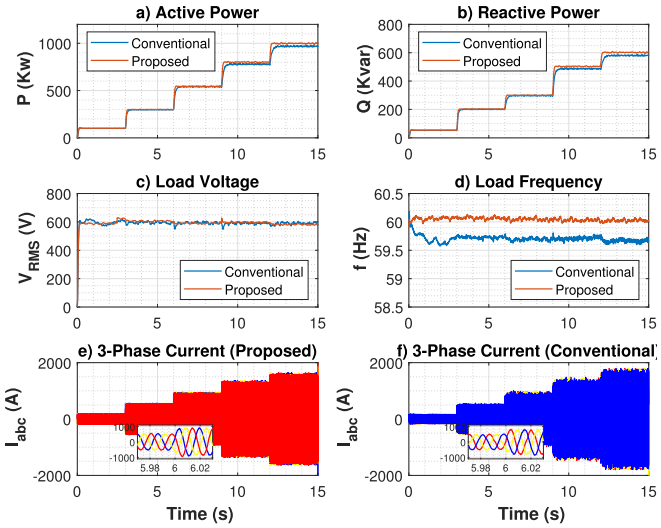

FIGURE 8. PHIL experimental results for 1MW system at IS mode.

and voltage. Fig. 6(e), (f) show the inverter output 3-phase current variation under load changes for both methods.

2) 100KW SYSTEM

In this test, the active power of the load is stepped up from zero till 100KW through 10KW, 50KW, Fig. 7(a). In addition, Fig. 7(b) demonstrates that the reactive power reaches 53KVAR after overrun from zero to 8KVAR, and 33KVAR. In islanded systems, the main electrical parameters that need to be monitored and investigated are the voltage and frequency curves. Therefore, Fig. 7(c), (d) present the voltage and frequency variations during the test period and confirm the proposed control technique's capability to supply the load at the nominal system parameters with less deviation than the conventional method. Also, the load current, inverter output current, for the proposed and conventional methods are plotted in Fig. 7(e), (f), respectively.

3) 1MW SYSTEM

To confirm the universality concept of the CFNN method, the 1MW system is presented in this part. The load active/reactive power are modified into five stages, 100KW/55KVAR, 300KW/200KVAR, 550KW/300KVAR, 800KW/500KVAR, and 1000KW/600KVAR, as shown in Fig. 8. Moreover, Fig. 8(d), load frequency, confirms that the proposed methodology can track the reference frequency at any load values while the conventional method cannot do the same. Besides, the proposed method shows more rigid load voltage stabilization than the benchmark method, as shown in Fig. 8(c). It is noteworthy that the drops in the frequency and voltage push the load to consume less active and reactive power. This effect is clearly noticed on the load 3-phase current, inverter output current, as depicted in Fig. 8(e), (f).

D. GRID-CONNECTED MODE

The proposed model along with the conventional model are also confirmed within the multi-inverter parallel connected and swing bus grid-connected scenarios. These test scenarios verify the robustness of the CFNN method to be used in general Microgrid applications.

1) MICROGRID MODEL

In this scenario, the three BESSs (10KW, 100KW, and 1MW) are connected in parallel to supply a variable load. The 1MW system is assigned a reference bus and the other two systems (10KW, 100KW) are used in grid-connected operating mode. During this test, the load is varied into Stage1: 200KW/100KVAR, Stage2: 600KW/200KVAR, and Stage3: 1000KW/400KVAR. During Stage1, the reference power of the 10KW system is 10KW/10KVAR, and that of the 100KW system is 100KW/90KVAR and 25KW/40KVAR. In the second stage, the reference power of 10KW and 100KW systems are 5KW/4KVAR and -50KW/10KVAR, respectively. While in the last stage, Stage3, the 10KW system's reference power is stepped up to 8KW/6KVAR, 9KW/8KVAR, and 10KW/10KVAR; also, the 100KW system's reference power is changed to 75KW/-40KVAR, 100KW/20KVAR, and 50KW/40KVAR. Fig. 9 presents the active/reactive power, voltage, and frequency for the load, 10KW, 100KW, and 1MW systems during this test scenario. From Fig. 9, the 1MW system compensates for the supplied power from 10KW, and 100KW systems to cover the required load power, and follows the active/reactive power variations generated from these two systems.

The negative active power means that the BESS acts as a load, charging the battery, and the negative reactive power operates the BESS as a reactive power load. Even more, the proposed method shows less oscillation in the load voltage than the conventional method, Fig. 9(e); while the load frequencies are almost the same in both methods, Fig. 9(f).

2) UTILITY GRID MODEL

During this scenario, the voltage source inverters along with the BESSs are operated in parallel with a swing bus.

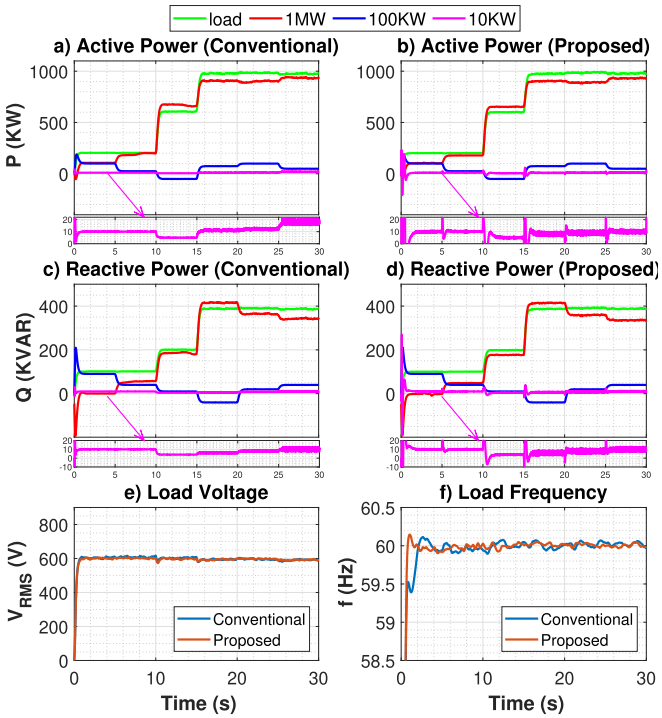

FIGURE 9. PHIL experimental results for 10KW, 100KW, 1MW systems at Microrid model.

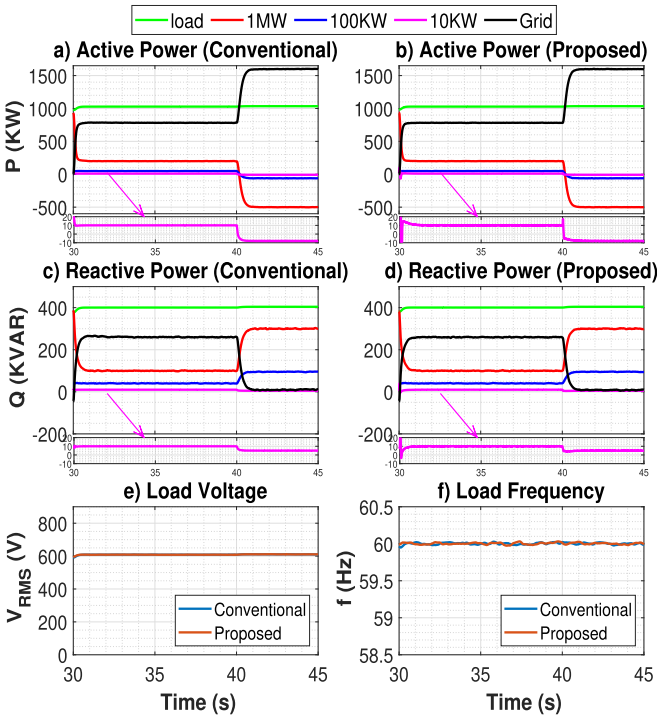

FIGURE 10. PHIL experimental results for 10KW, 100KW, 1MW systems at Utility Grid model.

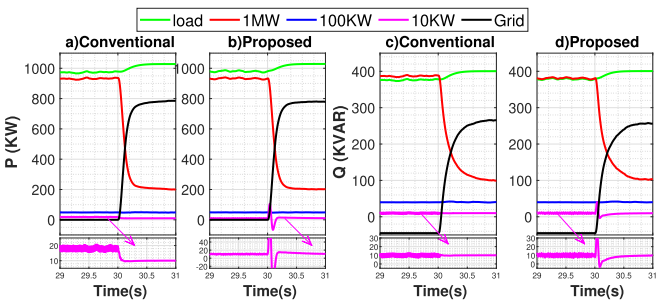

FIGURE 11. Active and reactive power for 10KW, 100KW, 1MW systems during dynamic transition.

All BESSs are controlled in grid-connected mode to share the load per the active/reactive power reference values. The load power is kept fixed at 1000KW/400KVAR while the BESSs' reference power values are varied into two stages. In the first stage, the 10KW, 100KW, and 1MW systems reference power are assigned to 10KW/10KVAR, 50KW/40KVAR, and 200KW/100KVAR, respectively. In contrast, the grid supplies the load by 740KW/250KVAR. In the second stage, the BESSs are in charging mode; the reference power values are -8KW/5KVAR, -60KW/95KVAR, and -500KW/300KVAR, which makes the grid the primary active power source, 1568KW. Fig. 10 shows the active and reactive power shared from the BESSs and swing grid during the test scenario. The load/systems voltage and frequency, Fig. 10(e), (f), follow the grid values to keep the systems synchronized with the grid over the stages of this scenario.

Besides, Fig. 11 presents the active and reactive power for 10KW, 100KW, and 1MW systems during the transition from islanded mode to grid-connected mode (Microgrid model to Utility Grid model). At the transition point of 30 sec, the grid switch is closed, and the state input of the 1MW system is switched to grid-connected mode. Fig. 11 shows that the dynamic transition effect clearly appeared in the 10KW system rather than in the other systems. While the 10KW system has high grid-side impedance; therefore, this impedance needs to be varied to increase the accuracy of the active/reactive power sharing and minimize the circulating current during the transient state. Hence, the virtual impedance strategy is one of the solutions to avoid the dynamic transition states [41]. Otherwise, in the conventional method, the power and current control loops play the main roles in the stability during dynamics with the limitation of the system parameters. At some points and before the transition from islanded mode to grid-connected mode at full load, the conventional method cannot keep up with the nominal system's size. The shared power goes over 10KW and 100KW. Thus, the proposed CFNN method shows more robustness against the reference/load power changes.

Remarkably, the load/reference active/reactive power variations, the nominal frequency/voltage tracking, and the operating mode lead to an instantaneous modulation in v_{dq} voltages. The proposed control method is capable of providing a rapid response to unpredicted changes in the power flow or operational mode. Since this strategy uses an online weight adaption technique over the q and d axes voltages and frequency, it has the benefit of a uniform and fast dynamical reaction. Also, using the per-unit values for training and reference parameters makes the proposed technique universal and applicable to any system size without extra tuning.

V. CONCLUSION

A cascade-forward neural network control approach has been devised for bi-directional inverter-based microgrids. A robust control technique is implemented using a multi-layer cascade-forward back-propagation scheme with online weight adaptation. The CFNN has three hidden layers of twenty-four, sixteen, and eight neurons each, next to three neurons in the output layer. Furthermore, the proposed technique is based on the CFNN structure and the mathematical model of the microgrid droop control theory. Combining these two strategies ensures that BESSs or distributed generation systems provide the necessary energy to the load or grid. As a result, the required active/reactive power is delivered to the load, maintaining the system's voltage and frequency under the islanded mode. The reference active/reactive power is also tracked at the bus voltage and frequency values under grid-connected mode. Besides, the proposed approach is generalized to operate a wide range of VSI systems without any further tuning. The performance of the suggested process is investigated in numerous phases for various scenarios using real-time PHIL experimental tests. The PHIL setup is created using a MATLAB/Simulink real-time environment and an Opal-RT system. The *OP*4510 system is used to drive the inverter bridge for testing the 10KW, 100KW, and 1MW BESSs. The fact that the neural network is trained offline brings more added value since it reduces the enormous computing load associated with such conventional approaches, along with the online weight adaptation technique assures tracking performance. Finally, the experimental results demonstrate the effectiveness of the developed control technique in both operating modes. Actually, the proposed method shows some deviation during dynamic transition and counts on the state signal for the operating mode (IS or GC). Thus, future work will try to investigate and analyze the transient state performance improvement for the CFNN control technique and avoid using the state input by relying on the actual measured values.

REFERENCES

[1] M. H. Saeed, W. Fangzong, B. A. Kalwar, and S. Iqbal, "A review on microgrids' challenges & perspectives," *IEEE Access*, vol. 9, pp. 166502–166517, 2021.

[2] S. Parhizi, H. Lotfi, A. Khodaei, and S. Bahramirad, "State of the art in research on microgrids: A review," *IEEE Access*, vol. 3, pp. 890–925, 2015.

[3] M. Ahmed, L. Meegahapola, A. Vahidnia, and M. Datta, "Stability and control aspects of microgrid architectures—A comprehensive review," *IEEE Access*, vol. 8, pp. 144730–144766, 2020.

[4] D. E. Olivares *et al.*, "Trends in microgrid control," *IEEE Trans. Smart Grid*, vol. 5, no. 4, pp. 1905–1919, Jul. 2014.

[5] J. Hu, Y. Shan, K. W. Cheng, and S. Islam, "Overview of power converter control in microgrids—Challenges, advances, and future trends," *IEEE Trans. Power Electron.*, vol. 37, no. 8, pp. 9907–9922, Aug. 2022.

[6] J. M. Guerrero, J. C. Vasquez, J. Matas, L. G. de Vicuna, and M. Castilla, "Hierarchical control of droop-controlled AC and DC microgrids—A general approach toward standardization," *IEEE Trans. Ind. Electron.*, vol. 58, no. 1, pp. 158–172, Jan. 2011.

[7] M. Velasco, C. Alfaro, A. Camacho, A. Borrell, and P. Martí, "Complex power sharing is not complex," *IEEE Trans. Smart Grid*, vol. 13, no. 3, pp. 1762–1773, May 2022.

[8] J. Rocabert, A. Luna, F. Blaabjerg, and P. Rodríguez, "Control of power converters in AC microgrids," *IEEE Trans. Power Electron.*, vol. 27, no. 11, pp. 4734–4749, Nov. 2012.

[9] E. Espina, J. Llanos, C. Burgos-Mellado, R. Cárdenas-Dobson, M. Martínez-Gómez, and D. Sáez, "Distributed control strategies for microgrids: An overview," *IEEE Access*, vol. 8, pp. 193412–193448, 2020.

[10] A. Gupta, S. Doolla, and K. Chatterjee, "Hybrid AC–DC microgrid: Systematic evaluation of control strategies," *IEEE Trans. Smart Grid*, vol. 9, no. 4, pp. 3830–3843, Jul. 2018.

[11] A. Mohammed, S. S. Refaat, S. Bayhan, and H. Abu-Rub, "AC microgrid control and management strategies: Evaluation and review," *IEEE Power Electron. Mag.*, vol. 6, no. 2, pp. 18–31, Jun. 2019.

[12] N. Mohammed, A. Lashab, M. Ciobotaru, and J. M. Guerrero, "Accurate reactive power sharing strategy for droop-based islanded AC microgrids," *IEEE Trans. Ind. Electron.*, early access, Apr. 19, 2022, doi: 10.1109/TIE.2022.3167141.

[13] A. Firdaus and S. Mishra, "Mitigation of power and frequency instability to improve load sharing among distributed inverters in microgrid systems," *IEEE Syst. J.*, vol. 14, no. 1, pp. 1024–1033, Mar. 2020.

[14] J. Schiffer, T. Seel, J. Raisch, and T. Sezi, "Voltage stability and reactive power sharing in inverter-based microgrids with consensus-based distributed voltage control," *IEEE Trans. Control Syst. Technol.*, vol. 24, no. 1, pp. 96–109, Jan. 2016.

[15] D. Rimorov, J. Huang, C. F. Mugombozi, T. Roudier, and I. Kamwa, "Power coupling for transient stability and electromagnetic transient collaborative simulation of power grids," *IEEE Trans. Power Syst.*, vol. 36, no. 6, pp. 5175–5184, Nov. 2021.

[16] Y. Sun, X. Hou, J. Yang, H. Han, M. Su, and J. M. Guerrero, "New perspectives on droop control in AC microgrid," *IEEE Trans. Ind. Electron.*, vol. 64, no. 7, pp. 5741–5745, Jul. 2017.

[17] S. Khanabdal, M. Banejad, F. Blaabjerg, and N. Hosseinzadeh, "Adaptive virtual flux droop control based on virtual impedance in islanded AC microgrids," *IEEE J. Emerg. Sel. Topics Power Electron.*, vol. 10, no. 1, pp. 1095–1107, Feb. 2022.

[18] F. Chen, R. Burgos, D. Boroyevich, J. C. Vasquez, and J. M. Guerrero, "Investigation of nonlinear droop control in DC power distribution systems: Load sharing, voltage regulation, efficiency, and stability," *IEEE Trans. Power Electron.*, vol. 34, no. 10, pp. 9404–9421, Oct. 2019.

[19] H. Shadabi and I. Kamwa, "Dual adaptive nonlinear droop control of VSC-MTDC system for improved transient stability and provision of primary frequency support," *IEEE Access*, vol. 9, pp. 76806–76815, 2021.

[20] Y. Zhang, X. Qu, M. Tang, R. Yao, and W. Chen, "Design of nonlinear droop control in DC microgrid for desired voltage regulation and current sharing accuracy," *IEEE J. Emerg. Sel. Topics Circuits Syst.*, vol. 11, no. 1, pp. 168–175, Mar. 2021.

[21] T. D. Raoult, I. Kamwa, T. Jacques, and C. F. Mugombozi, "Supervised learning of overcomplete dictionaries for rapid response-based dynamic stability prediction," *IEEE Trans. Power Syst.*, early access, Mar. 3, 2022, doi: 10.1109/TPWRS.2022.3156025.

[22] K. Shi, H. Ye, W. Song, and G. Zhou, "Virtual inertia control strategy in microgrid based on virtual synchronous generator technology," *IEEE Access*, vol. 6, pp. 27949–27957, 2018.

[23] X. Meng, J. Liu, and Z. Liu, "A generalized droop control for grid-supporting inverter based on comparison between traditional droop control and virtual synchronous generator control," *IEEE Trans. Power Electron.*, vol. 34, no. 6, pp. 5416–5438, Jun. 2019.

[24] J. Liu, Y. Miura, and T. Ise, "Comparison of dynamic characteristics between virtual synchronous generator and droop control in inverter-based distributed generators," *IEEE Trans. Power Electron.*, vol. 31, no. 5, pp. 3600–3611, May 2016.

[25] C. F. Mugombozi, J. Mahseredjian, and O. Saad, "Efficient computation of feedback-based control system equations for electromagnetic transients," *IEEE Trans. Power Del.*, vol. 30, no. 6, pp. 2501–2509, Dec. 2015.

[26] A. A. Eajal, A. H. Yazdavar, E. F. El-Saadany, and M. M. A. Salama, "Optimizing the droop characteristics of AC/DC hybrid microgrids for precise power sharing," *IEEE Syst. J.*, vol. 15, no. 1, pp. 560–569, Mar. 2021.

[27] A. A. Derbas, M. Kheradmandi, M. Hamzeh, and N. D. Hatziargyriou, "A hybrid power sharing control to enhance the small signal stability in DC microgrids," *IEEE Trans. Smart Grid*, vol. 13, no. 3, pp. 1826–1837, May 2022.
[28] F.-J. Lin, K.-H. Tan, C.-F. Chang, M.-Y. Li, and T.-Y. Tseng, "Development of intelligent controlled microgrid for power sharing and load shedding," *IEEE Trans. Power Electron.*, vol. 37, no. 7, pp. 7928–7940, Jul. 2022.
[29] H. R. Baghaee, M. Mirsalim, and G. B. Gharehpetian, "Power calculation using RBF neural networks to improve power sharing of hierarchical control scheme in multi-DER microgrids," *IEEE J. Emerg. Sel. Topics Power Electron.*, vol. 4, no. 4, pp. 1217–1225, Dec. 2016.
[30] M. Parvizimosaed and W. Zhuang, "Enhanced active and reactive power sharing in islanded microgrids," *IEEE Syst. J.*, vol. 14, no. 4, pp. 5037–5048, Dec. 2020.
[31] Y. Mi, H. Zhang, Y. Fu, C. Wang, P. C. Loh, and P. Wang, "Intelligent power sharing of DC isolated microgrid based on fuzzy sliding mode droop control," *IEEE Trans. Smart Grid*, vol. 10, no. 3, pp. 2396–2406, May 2019.
[32] P. Liu, Y. Bi, and C. Liu, "Data-based intelligent frequency control of VSG via adaptive virtual inertia emulation," *IEEE Syst. J.*, vol. 16, no. 3, pp. 3917–3926, Sep. 2022.
[33] R. T. Dabou, I. Kamwa, C. Y. Chung, and C. F. Mugombozi, "Time series-analysis based engineering of high-dimensional wide-area stability indices for machine learning," *IEEE Access*, vol. 9, pp. 104927–104939, 2021.
[34] D.-D. Zheng, S. S. Madani, and A. Karimi, "Data-driven distributed online learning control for islanded microgrids," *IEEE J. Emerg. Sel. Topics Circuits Syst.*, vol. 12, no. 1, pp. 194–204, Mar. 2022.
[35] K. Hornik, "Approximation capabilities of multilayer feedforward networks," *Neural Netw.*, vol. 4, no. 2, pp. 251–257, 1991. [Online]. Available: https://www.sciencedirect.com/science/article/pii/089360809190009T
[36] M. Alzayed, H. Chaoui, and Y. Farajpour, "Maximum power tracking for a wind energy conversion system using cascade-forward neural networks," *IEEE Trans. Sustain. Energy*, vol. 12, no. 4, pp. 2367–2377, Oct. 2021.
[37] M. D. O. Faruque *et al.*, "Real-time simulation technologies for power systems design, testing, and analysis," *IEEE Power Energy Technol. Syst. J.*, vol. 2, no. 2, pp. 63–73, Jun. 2015.
[38] C. Dufour, J. Mahseredjian, J. Bélanger, and J. L. Naredo, "An advanced real-time electro-magnetic simulator for power systems with a simultaneous state-space nodal solver," in *Proc. IEEE/PES Transm. Distrib. Conf. Expo. Latin America (TD-LA)*, 2010, pp. 349–358.
[39] C. Dufour, J. Mahseredjian, and J. Bélanger, "A combined state-space nodal method for the simulation of power system transients," *IEEE Trans. Power Del.*, vol. 26, no. 2, pp. 928–935, Apr. 2011.
[40] C. Rabbath, M. Abdoune, and J. Belanger, "Effective real-time simulations of event-based systems," in *Proc. Winter Simulat. Conf.*, vol. 1, 2000, pp. 232–238.
[41] M. Ahmed, L. Meegahapola, A. Vahidnia, and M. Datta, "Adaptive virtual impedance controller for parallel and radial microgrids with varying X/R ratios," *IEEE Trans. Sustain. Energy*, vol. 13, no. 2, pp. 830–843, Apr. 2022.

MOHAMAD ALZAYED (Member, IEEE) received the Ph.D. degree in electrical and computer engineering from Carleton University, Ottawa, ON, Canada. His career has bridged both academia and industry with more than 14 years of experience in control and electrical energy resources, grid management and efficiency, electrical design and contracting, and project management. Since 2019, he has been a member with the Intelligent Robotic and Energy Systems Research Group, Department of Electronics, Carleton University and joined the Laboratory of Signal and System Integration, Department of Electrical and Computer Engineering, University of Quebec at Trois-Rivières, in 2022. His teaching/research activities focus on intelligent control of electric machines and power converters for energy systems, real-time simulations, and power systems. He is a Guest Editor of several journals.

MICHEL LEMAIRE received the B.S. and M.S. degrees in electrical engineering from the Electrical Energy Engineering Institute, University of Quebec Trois-Rivières (UQTR), Trois-Rivières, QC, Canada, in 2014 and 2017, respectively, where he is currently pursuing the Ph.D. degree in electrical engineering; the thesis focuses on the FPGA implementation of electric circuit solvers for real-time applications. His research interests include power hardware-in-the-loop and hardware-in-the-loop simulation systems, real-time simulation, electric circuit modeling and solving, control and power electronics, motor and grid emulation, four quadrant amplifier design, and low latency inter-FPGA communication.

SINA ZARRABIAN (Member, IEEE) received the Ph.D. degree in electrical engineering from Tennessee Technological University, Cookeville, TN, USA, in 2016. He is currently an Associate Professor with the Department of Electrical Engineering, The State University of New York, Maritime College, Throggs Neck, NY, USA. His research interests include power system dynamics and stability, wide-area monitoring and control of power systems, smart grids, and microgrids.

HICHAM CHAOUI (Senior Member, IEEE) received the Ph.D. degree in electrical engineering from the University of Quebec, Trois-Rivières, QC, Canada, in 2011. His career has spanned both academia and industry in the field of control and energy systems. From 2007 to 2014, he held various engineering and management positions with Canadian industry. He is currently an Associate Professor with Texas Tech University, TX, USA, and also with Carleton University, Ottawa, ON, Canada. His scholarly work has resulted in more than 150 journal and conference publications. He was the recipient of the Best Thesis Award, the Governor General of Canada Gold Medal Award, the Carleton's Research Excellence Award, the Early Researcher Award from the Ministry of Colleges and Universities, and the Top Editor Recognition from IEEE Vehicular Technology Society. He is a Registered Professional Engineer in the province of Ontario and an Associate Editor of several IEEE journals.

DANIEL MASSICOTTE (Senior Member, IEEE) received the B.Sc.A. and M.Sc.A. degrees in electrical engineering and industrial electronics from the Université du Québec à Trois-Rivières, Trois-Rivières, QC, Canada, in 1987 and 1990, respectively, and the Ph.D. degree in electrical engineering from the École Polytechnique de Montréal, Montréal, QC, Canada, in 1995. In 1994, he joined the Department of Electrical and Computer Engineering, Université du Québec à Trois-Riviéres, where he is currently a Full Professor. He is the Founder of the Laboratory of Signal and Systems Integration. Since 2001, he has been the Founding President and a Chief Technology Officer of Axiocom Inc. He was the Head of the Industrial Electronic Research Group from 2011 to 2018 and the Head of the Electrical and Computer Engineering Department since 2014. He is also the Head of the Research Chair in Signals and Intelligence of High-Performance Systems. He is the author/coauthor of more than 200 technical papers in international conferences and journals, as well as of nine inventions. His research interests include advanced VLSI implementation, digital signal processing for wireless communications, measurement, medical, real-time simulation and control problems for linear/nonlinear complex systems. He has proposed many methods based on modern signal processing such as machine learning, transform domain, and metaheuristics. He received the Douglas R. Colton Medal for Research Excellence awarded by the Canadian Microelectronics Corporation, the PMC-Sierra High Speed Networking and Communication Award, and the Second place at the Complex Multimedia/Telecom IP Design Contest from Europractice. He is also a member of the "Ordre des Ingénieurs du Québec" and "Microsystems Strategic Alliance of Quebec" (ReSMiQ).